
Article:
Noor, F, Vorozhtsov, A, Lerner, M et al. (2015) Thermal-Chemical Characteristics of Al-Cu Alloy Nanoparticles. JOURNAL OF PHYSICAL CHEMISTRY C, 119 (25). pp. 14001-14009. ISSN: 1932-7447

https://doi.org/10.1021/acs.jpcc.5b01515

Thermal-Chemical Characteristics of Al-Cu Alloy Nanoparticles

Fahad Noor[1], Alexander Vorozhtsov[2], Marat Lerner[3], Enio Bandarra Filho[4], Dongsheng Wen[6]*

[1] Department of Mechanical Engineering, University of Engineering and Technology, Lahore, Pakistan

[2] School of Physics, Tomsk State University, Tomsk, Russia

[3] Institute of Strength Physics and Material Science, Russia Academy of Science, Tomsk, Russia

[4]School of Mechanical Engineering, Federal University of Uberlandia, Brazil

[5]School of Chemical and Process Engineering, University of Leeds, Leeds, UK

Corresponding author (D Wen) E-mail: d.wen@leeds.ac.uk ; Tel: 0044 113 3431299; Address: School of Chemical and Process Engineering, University of Leeds, Leeds, UK

Abstract: This work investigated the oxidation, ignition and thermal reactivity of alloy nanoparticles of aluminum and copper (nAlCu) using simultaneous thermogravimetric analysis (TGA) and differential scanning calorimeter (DSC) method. The microstructure of the particles was characterized with scanning electron microscope (SEM) and transmission electron microscope (TEM), and the elemental composition of the particles before and after the oxidation was investigated with energy dispersive X-ray spectroscopy (EDS) and X-ray diffraction (XRD). The particles were heated from room temperature to 1200 ^{o}C under different heating rates from 2 to 30 K/min in the presence of air. The complete oxidation process of the nAlCu was characterized by two exothermic and two endothermic reactions, and the reaction paths up to 1200^{o}C were proposed. An early ignition of nAlCu, in the temperature around 565^{o}C, was found at heating rates ≥ 8 K/min. The eutectic melting temperature of nAlCu was identified at ~ 546^{o}C, which played a critical role in the early ignition. The comparison of the reactivity with that of pure Al nanoparticles showed that the nAlCu was more reactive through alloying.

Keywords: Alloys, nanoparticles, energetic materials, TGA, DSC, oxidation, ignition, aluminum copper oxides, nanofuel.

1. Introduction

Metal based energetic materials (EMs) have been used in many applications including thermites, metastable intermolecular composites (MICs), explosives, pyrotechnics, composite solid propellants and energy storage [1-4]. Aluminum is a favorite choice because of its high reaction enthalpy, abundance, low cost and technological maturity for manufacturing. However for many of these applications, the high theoretical combustion enthalpy of aluminum could not be practically achieved within the required time periods due to long metal ignition delays, particles agglomeration before ignition, slow burning rates and incomplete combustion[5-6]. Powders of metastable aluminum-based alloys have been proposed to address these problems in order to increase burning rates [6-8]. Interesting physicochemical properties would be obtained for alloy particles through chemical reordering and spatial redistribution of constitutional atoms [9]. While the overall combustion enthalpy would not be affected significantly, the exothermic phase changes occurring on the metastable relaxation of such alloys would result in the decomposition of the supersaturated solid solutions and formation of intermetallic phases. This would accelerate the reaction kinetics, leading to early ignition and increased overall combustion rates[7,8].

A few studies have been conducted to investigate the thermo-mechanical and chemical activities of aluminum based alloy particles. For instance Shoshin et al. examined the ignition and combustion characteristics of aluminum rich Al-Ti, Al-Mg and Al-Li particles (10-14μm) [7-8]. It was found that the flame speed of the alloy aerosol was higher than those produced by Al, Ti and Mg aerosols individually, and the ignition temperature of the alloy was decreased with the increase of the concentration of Ti or Mg. Wang et al. [10] showed that with the increase of Mg concentration, the brittleness of the Al-Mg alloy particles (0.75μm-6.64μm) increased, and the particles were ignited at ~ 620^{o}C, even lower than the theoretical melting temperature (660^{o}C) of aluminum. The amount of heat produced and the weight increased had a direct linkage with the

composition of the alloy. For these micrometer-sized alloy particles, the main tool to modify particle property is to vary their constitutional compositions, which has its own limitations. At the nanoscale, however, the properties become strongly reliant on the particle morphology due to the large specific surface areas. The particle properties can be consequently tuned and engineered to meet specific requirements by varying elemental compositions, internal structures, and particle morphology [11-13]. For metal-metal oxides alloys, many studies have shown that decreasing particle size to the nanoscale could reduce the ignition delay and improve the combustion rates of MICs and other aluminum-based energetic formulations [14-18]. For bi-metal alloy nanoparticles, however, there is only very limited investigations, partly due to the difficulties of producing well-controlled metallic alloy particles [19]. Limited quantities of Ni-Cu, Ni-Co and Ni-Zn alloy nanoparticles were produced by hydrazine reduction of metal chloride in ethylene glycol by Singh et al. [20], and a clear reduction in the ignition delay was observed. However there is still no detailed study of the thermal-chemical kinetics of bimetallic alloy nanoparticles, especially Al-Cu, and their properties in relation to the bulk behavior and individual compositional elements are still unclear.

In this work, Al-Cu alloy nanoparticles (nAlCu) were produced through an improved Electric Explosion of Wire (EEW) method, and the oxidation and ignition behavior of nAlCu in the atmosphere of air were investigated with by the thermo-gravimetric analysis (TGA) and differential scanning calorimeter (DSC). The reactivity and stability of the alloy nanoparticles at various temperatures and heating rates were studied, and compared with that of aluminum particles of similar dimensions. The microstructure and morphology of the powder were characterized by a transmission electron microscope (TEM) and a scanning electron microscope (SEM), and the chemical and structural analysis of the products of various oxidation steps were investigated by X-ray diffraction (XRD).

2. Experimental methods

2.1 Material production

A few methods have been used to produce alloy nanoparticles, i.e, chemical/electrochemical/sono-chemical synthesis, ion implantation and thermal decomposition [19], which however usually have the problems of impurities and small quantities. In this work, alloy nanoparticles were fabricated by the electrical explosion of wires (EEW) method, which is a process of explosive destruction of a metal wire under the action of high density current. It has been successfully used to produce various pure metal and metal oxide particles such as Al, Fe, Ni, Si and Fe_2O_3 [20-24], as well as a few alloy nanoparticles (i.e., Al-Cu, Al-Ni) [25]. For alloy particles, coated metal wires were generally used where one metal component was electrodeposited onto the surface of another metal wire and EEW was subsequently applied [25]. A new approach was used in this work to circumvent the process of electrodeposition by simultaneously electrical explosion of two-twisted metal wires, Fig. 1. In this process, the constitutional elements of Al and Cu were twisted in wires and put in the production chamber. The aluminum content in the explosion products was adjusted by varying its wire diameter. The chamber was vacuumed and filled by argon gas at a pressure of $3x10^5$ Pa. A high voltage power unit charged a capacitor bank, which discharged a high current in the order of 10^5 A/mm^2 to the wires in a burst (i.e. 10^{-5}-10^{-8} s), resulting in rapid boiling and evaporation of the wires. The energy characteristics of EEW were calculated by a current oscillogram, obtained through the current sensor according to the Kvartzkhava method [26]. The mixtures of superheated vapor and boiling droplets of the exploding wires were subsequent condensed in argon gas. The particles were collected, passivated in inert atmosphere by slow gas puffing for three days, and then stored in sealed vacuum packages. The nanoparticle production rate is dependent on the diameters of the wires, and is in the range of 70 - 100 g/hour. In principle, different compositions of nAlCu

particles could be produced by varying the initial wire diameter, and an aluminum to copper mass ratio of 4:1 (molar ratio, 9.4:1) was used for this study.

2.2 Material characterization

The particle size distribution (PSD) and the mean diameter of alloy nanoparticles were characterized by a Nanosizer (Malvern, UK), based on the principle of dynamic light scattering (DLS). Before the DLS, the particles were dispersed in the liquid medium of hexane and sonicated to reduce particle agglomeration. The particle shapes before and after the experiments were determined by a SEM (Inspect F, FEI Company, EU) operated at 10 kV. The elemental compositional analysis was performed by an Energy Dispersive X-ray Spectrometer (EDS) (Oxford Instruments) equipped with INCA Energy 300 Systems. The microstructure and initial oxide layer was examined by a high resolution transmission electron microscope (HRTEM, - JEOL JEM 1020) operated at 200 kV. Before the TEM, the sample particles were dispersed in the solution of ethanol and de-agglomerated in a ultrasonic bath for five minutes, and carbon coated grids were used.

The oxidation and ignition of nAlCu at different temperature ranges were investigated by a STA 1500 thermal analyzer (Rheometric Scientific, Germany) in a controlled atmosphere of dry air at a flow rate of 20 ml/min, similar to our previous studies [27-30]. The weight gain during the oxidation process was measured using TGA while the heat absorbed / released during the endothermic or exothermic processes respectively was obtained from DSC plots. The temperature of the TGA was calibrated against the melting points of metals such as Zn, Sn and Pb. For all experiments, platinum crucibles that are inert to nAlCu within the experimental range were selected and small sample quantities were used, i.e., 6.1 ± 0.1 mg, to reduce the tendency of developing an internal temperature gradient inside the crucible. Two sets of experiments were

performed to investigate the effect of heating rate on the oxidation kinetics and the thermal stability of the samples. In the first set, the samples were thermally oxidized from room temperature to 1200 ^{o}C at heating rates of 2, 5, 7, 10, 15, 20, 30 K/min respectively. In the second set, a fixed heating rate of 10 K/min was used and the experiments were terminated at some characteristic temperature points, i.e., 570 ^{o}C, 900 ^{o}C, 1100 ^{o}C, and 1200 ^{o}C, to reveal crystal structures and reaction pathways. The products of all these experimentations were cooled in nitrogen gas and preserved for crystalline structure analyses. Ex-situ powder X-ray diffraction analysis (Siemens, D500 Diffractometer) was performed at 40 kV and 40 mA using CuKα radiation (λ =0.15418nm) and the diffraction pattern from 10^{o} to 70^{o} (2θ) of each product was recorded to identify different phase compositions.

3. Results and discussion

3.1 Particle size, morphology, and phase composition

The TEM image, **Fig. 2a**, shows that the primary particles were spherical in shape and have a relatively uniform size distribution in the range of 30 ~ 120 nm. The thickness of the oxide passivation layer was identified ~ 3.2 nm. **Fig. 2b** shows the particle size measurement by DLS, which had a mono-modal distribution with a polydispersity index of 0.33. The peak diameter was 211 nm with a Z-average diameter of 343 nm and a width of 95.8 nm. The difference to the TEM results are due to the nature of the DLS measurement, which measures the hydrodynamic diameter in a liquid medium where particle agglomerations are inevitable. The elementary map, **Fig. 3**, shows that Al, Cu and O were uniformly distributed. The presence of O was due to the formation of the passivation layer and was in the form of oxide. The content of the constitutional elements, detected by the EDS, are given in Table 1. Depending on the sampling position, Cu content varied from 17% to 25%, and four sampled average of Cu ratio was ~21%, consistent with the initial copper content used for EEW by assuming the initial oxide layer as alumina. The

decreased Al element (~58%) from the original composition suggests that the passivation layer of nAlCu was in the form of Al-O. XRD analysis shows that no oxide peak was detected in the diffractogram diagram, which confirms that the passivation oxide was in the amorphous phase. It also shows that the sample contained pure Al (JCPDS card no. 04-0787), and two intermetallic compounds of $CuAl_2$ (JCPDS card no. 250012) and Cu_9Al_4 (JCPDS card no. 24-0003).

3.2 Thermal analysis and reaction kinetics

Thermal characteristics such as thermal reactivity, ignition temperature, peak temperatures of various physicochemical reactions of nAlCu were evaluated by TGA/DSC. During the experimentation, the sample's weight gain and heat flow were recorded simultaneously. It is observed that the heat flow pattern changed significantly with the heating rates. The experiments fall into two distinct types: low heating rate (β = 2-7 K/min) and high heat rate ($\beta \geq 8$ K/min). For the low heating rate, the oxidation process completes without any sudden change of heat or mass. For the high heating rate, there is a sudden increase of mass and heat flow, indication of an early ignition. Both oxidation types have some distinctive features and are explained separately.

Fig.4 shows simultaneous the TGA/DSC curve at a heating rate of 7 K/min. The reaching of the plateau at the high temperature (i.e. >1000 ^oC) shows that the oxidation process was fully completed. The slight decrease of the sample mass to point 'a' (450 ^oC) was due to the desorption of the adsorbed moisture and CO_2 in the sample [31]. The first exothermic process started at 525 ^oC, peaked at 547.8 ^oC and ended at 590 ^oC. During the reaction, there was an increase of 18.1% in mass and a release of 2.3 kJ energy. The endothermic peak was observed at 591^oC, which was due to the peritectic reaction [32], as shown in the phase diagram of AlCu binary system in **Fig. 5**. The second exothermic process peaked at 755 ^oC, after which the reaction rate decreased and the sample went through an endothermic process. During this reaction, the weight of sample

increased linearly and the TGA trace became a straight line near 1000 ^{o}C. An increase of 30.8 % of the weight was shown in this reaction. At temperature ~ 1150^{o}C, the weight of the sample began to decrease (~ 4 %) till it reached the end of the experiment, T= 1200 ^{o}C. Similar oxidation scenario was observed for heating rates of 2-7 K/min, as shown in **Fig. 6**.

The simultaneous TGA/DSC curve at 10 K/min is taken as an example to illustrate the high heat rate case, **Fig. 7**, and all the TGA/DSC curves for heating rates of 10–30 K/min are shown in **Fig.8**. It can be observed that the onset temperature for the first exothermic reaction was ~500 ^{o}C and it completed ~ 560^{o}C. As the heating rate becomes ≥8K/min, the large amount of exothermic heat became far more than that could be absorbed by the purge gases, which resulted in a rapid increase in the particle temperature, **Fig 7**. Consequently the slope of heating rate (dT/dt) was shifted to a high value, which cannot be controlled by the programmed heating. The sample underwent a fast reaction with a sharp increase in the weight and a rapid release of heat in a very short period of time. This temperature run away has been regarded as the ignition point and is due to the self-heating of the particles [30, 33,34]. The nAlCu particle was identified as ~553^{o}C at the heating rate of 10 K/min. Similar to the observation from pure aluminum nanoparticles [30], such an ignition did not cause a global combustion event of the sample, but changed the characteristics of the following oxidation processes. To investigate further the early ignition reaction and chemical reaction pathways, another nAlCu sample was heated under the same heating rate to 570 ^{o}C (i.e., after the early ignition event) under the same conditions and then preserved in nitrogen gas. The end products were analyzed by XRD ex-situ, shown in **Fig. 9**. The peaks of δ-alumina (JCPDS card no. 04-0877) appeared on the radiograph at 2θ = 37.3^{o} and 45.9^{o}, and the main chemical reaction in the temperature span of 500^{o}C ~ 600^{o}C can be identified as,

$$4Al + 3O_2 \rightarrow \delta\text{–}2Al_2O_3 \quad (1)$$

During this reaction, 19.5 % of the mass was increased and 4.4 kJ/g of heat was produced. Like bulk metals, some mixtures of elements in alloys can be liquefied at a single invariant temperature called the eutectic temperature. The eutectic temperature for Al-Cu alloy in its bulk state is 548.2 ^{o}C, **Fig. 5**. Nearly the same value for nAlCu is found from the current experiment, 545.6 ^{o}C ±1.4^{o}C, **Fig. 8**. Immediately after the eutectic melting reaction, the particles went through the rapid exothermic reaction that led to the early ignition. For pure nAl, it has been suggested that the early ignition was associated with the melting and solid phase transition of alumina [30,35]. Under very high heating rates (i.e, >10^3 K/s), the melting of aluminium would fragmentize the shell and led to a global combustion event [36]. From the DSC/TGA data and the identified first-stage reaction, Eq.(1), it appears plausible that the melting of Al-Cu alloy nanoparticles played an important role in early ignition. Due to the eutectic melting of the alloy particle, the volume of the core increased, which created a high pressure on the alumina shell. This would increase the porosity of the surrounding shell or produce some cracks in preferred locations, exposing more un-reacted metal contents to the oxidizer, leading to the early ignition. However this early ignition was not strong enough to induce a global combustion of the alloy particle; the formed oxides would quickly seal the particles and reduced the diffusion rate of the oxygen, hence the reaction rate.

The second exothermic reaction started ~ 625 ^{o}C and reaches the maxima at 760^{o}C, after which the rate of energy release decreased constantly. The span of this reaction is wider as compared to the first reaction. During this reaction, the weight of the sample was increased by ~31.8 % until 1040 ^{o}C where the TGA trace became flat. To characterize this peak and the associated reactions, the particles were oxidized from room temperature to 900 ^{o}C and 1100 ^{o}C, and XRD are used to examine the oxidation products. The radiograph of the particles heated to 1100^{o}C was similar to that at 900 ^{o}C. From the XRD data and the analyses of the products at 900^{o}C, the peaks of copper

oxide CuO (JCPDS card no. 48-1548) and θ-Al_2O_3 (JCPDS card no. 11-0517) were identified. Various minor phase peaks of complex aluminum oxide such as copper aluminate spinel $CuAl_2O_4$ (JCPDS card no. 01-1153) produced by the chemical reactions between copper oxide and δ-, θ-alumina were also found, which is consistent with some early results [37-39].The main reaction paths in the temperature range of 600 ~ 1100 ºC can therefore be proposed as

$$\delta\text{-}Al_2O_3 \rightarrow \theta\text{-}Al_2O_3 \quad (2)$$

$$CuAl_2 + 2O_2 \rightarrow Al_2O_3 + CuO \quad (3)$$

$$Al_2O_3 + CuO \rightarrow CuAl_2O_4 \text{ (weak peaks)} \quad (4)$$

In the Cu-Al system, the formation of complex aluminum copper oxide at atmospheric pressure conditions, i.e., P_{O2}=0.21 atm, are generally observed at temperature above 1000 ºC [40]. Here we showed the existence of $CuAl_2O_4$ phase at ~900ºC, which should be associated with the increased reactivity at the nanoscale and the early ignition phenomenon ~560ºC. As the diffusion of metallic ions at 900 ºC was slow hence its formation was not favorable, which resulted in weak peaks observed (Eq. 4).

When the sample temperature was reached over 1150 ºC, its weight was decreased by ~ 4 %. Through XRD analysis, various phases of complex aluminum oxides were identified in the products. These oxides were produced by the chemical reactions between CuO and alumina. The radiograph shows the peaks of a variety of products, including Al, $CuAl_2$, CuO, $CuAl_2O_4$, α-Al_2O_3 (JCPDS card no. 46-1212) and Cu_2O (JCPDS card no. 35-1091). The peaks of multi oxide form of cuprous aluminate delafossite ($CuAlO_2$, JCPDS card no. 35-1401) were also observed. Hence the complicated ongoing reactions over 1100ºC can be proposed as,

$$\theta\text{-}Al_2O_3 \rightarrow \alpha\text{-}Al_2O_3 \quad (5)$$

$$Al_2O_3 + CuO \rightarrow CuAl_2O_4 \quad (6)$$

$$2CuAl_2O_4 \rightarrow 2CuAlO_2 + Al_2O_3 + 0.5O_2 \text{ (liberated)} \quad (7)$$

or

$$4CuO \rightarrow 2Cu_2O + O_2 \text{ (liberated)} \quad (8)$$

$$Cu_2O + Al_2O_3 \rightarrow 2CuAlO_2 \quad (9)$$

and

$$4CuAlO_2 + O_2 \rightarrow 2CuO + 2CuAl_2O_4 \quad (10)$$

$$4CuAlO_2 + 2Al_2O_3 + O_2 \leftrightarrow 4CuAl_2O_4 \quad (11)$$

According to the temperature-pressure phase fields boundaries of CuO-$CuAlO_2$-$CuAl_2O_4$ system [41], $CuAlO_2$ was thermodynamically stable in air only at T > 950 ^oC. Below this temperature, it transformed to $CuAl_2O_4$ following the pathway of Eq.(10). In the rich mixture of alumina, cuprous aluminate delafossite ($CuAlO_2$) was metastable in air between 1050 ^oC and 1170 ^oC and converted to copper aluminate spinel ($CuAl_2O_4$) following a reversible reaction (Eq. 11) [42,43]. The weight decrease at T > 1175 ^oC can be attributed to the oxygen produced during the reduction of CuO to Cu_2O as in the reaction Eq. (8) or Eq. (7).

The peaks of α-alumina have gained strength due to the crystallographic transformation of theta-alumina at high temperatures. Overlapping peaks of Cu_2O (JCPDS card no. 35-1091) with alumina and delafossite were also observed at 1200 ^oC, and the intensities of the peaks of $CuAl_2$ and Al were decreased with the increase of the temperature. No elemental Cu peaks were observed.

3.3 Reactivity comparison with nAl

It has been suggested that the reactivity of different particles can be estimated by the onset temperature, the peak temperature, and the temperatures at which the rate of change of mass and heat produced are the maximum [44,45]. The reactivity of nAlCu was compared with nAl having an average diameter of 150 nm in this section. It should be noted that particle sizes were slightly different due to the difficulties of fabricating nanoparticles with a close particle size matching. However a smaller size would suggest that the compared Al particle shall be more reactive than those having similar size as nAlCu. The comparative DSC/TGA example curves are shown in **Fig. 10**, where the particles were heated from room temperature to 700 ^{o}C. The reactivity parameters of both powders are summarized in **Table 2**. Among all the characteristic points compared, the temperatures of nAlCu were consistently smaller than those of nAl. For instance, the onset oxidation temperature of nAlCu was 528 ^{o}C, and it was 23 K earlier than that of nAl. This early reaction was believed to be related to the metastable relaxation of Al-Cu alloy that would result in the decomposition of the supersaturated solid solutions [8]. The early heat release would accelerate the following reaction kinetics. It is noted that the heat release of nAlCu was smaller than that of nAl, which shall be related to the smaller aluminium content in the alloy particle. Another caution should be paid is the influence of initial oxide layer. Based on the EDX analysis, the two samples had slight different initial oxide thickness. However the result from this work demonstrated clearly that nAlCu was more reactive than nAl at low heating rates.

For experiments conducted at high heating rate (i.e. $\beta \geq 8$ K/min), the ignition temperatures of both powders were compared, **Fig.11**. The ignition temperature was obtained by the 2nd derivative of TGA and DSC curves and the difference calculated by these two methods is in the range of ~ 1K. There is a general trend of the increase of ignition temperature with the increase of heating rate but the ignition temperature was consistently smaller for nAlCu. Regardless of the heating rate effect, the ignition temperature of nAlCu was 564.7±10.8 ^{o}C, which was similar to

that observed by Stamatis et al. in their study of ignition of Al-CuO nanocomposites [46]. The ignition temperature of nAl under similar experimental conditions was 595.5 ± 8.1°C. This again suggests that nAlCu was more reactive than nAl. Comparing with the melting temperature, it becomes clearer that the ignition of nAl occurred before the bulk melting of aluminium (i.e. T_m~660°C) whereas the ignition of nAlCu was after the melting (i.e., the eutectic melting temperature of AlCu alloy has similar values at the bulk and nano-alloy level, 545~548 °C). As discussed earlier, such an early melting of the alloy shall be responsible for the early ignition.

4. Conclusions

The oxidation, ignition and chemical kinetics of the Al-Cu alloy nanoparticles (nAlCu) were investigated in this work under different heating rates, from 2 to 30 K/min, up to 1200 °C in the presence of air. It can be concluded that:

- The complete oxidation scenario of nAlCu were characterized by two exothermic and two endothermic processes, associated with the melting and different reaction paths.
- An early ignition phenomenon was observed for nAlCu at heating rates $\beta \geq 8$ K/min, which was characterized with sudden change of mass and heat released, and the ignition temperature was identified in the region of 564.7 ± 10.8 °C .
- The eutectic melting temperature of nAlCu was found to be 545.6°C ± 1.4°C, similar to its bulk value, and played a critical role for the early ignition of aAlCu.
- The reaction paths at different oxidation stages up to 1200°C for nAlCu were proposed in conjunction with the XRD analysis.
- The comparison of reactivity and ignition temperature showed that nAlCu was more active than pure aluminium nanoparticles under similar experimental condition, showing increased reactivity through alloying.

Acknowledgement

The authors appreciate the support by the University of Engineering and Technology, Lahore under Faculty Development Programme (FDP) in collaboration with the Higher Education Commission (HEC) of Pakistan, and the support from The Program for Professor of Special Appointment (Eastern Scholar) at Shanghai Institutions of Higher Learning.

Reference

[1] S. Tanyir and Q Li. J. Propulsion and Power, 31 (2015): 408-415.

[2] Spitzer, D.; Risse, B.; Schnell, F.; et al Scientfic Report, 4 (2014), 6575

[3] R.W. Conner, D.D. Dlott. J. Physical Chemistry A, 114 (2010):6731-6741.

[4] D.S. Wen, Energy & Environmental Science 3 (2010):591-600.

[5] E.M. Hunt, M.L. Pantoya. J. Applied Physics 98 (2005):034909

[6] E.L. Dreizin Progr. Energy Combust. Sci., 26 (1) (2000): 57–78

[7] Y.L. Shoshin, E.L. Dreizin . AIAA Journal 42 (2004):1416-1426

[8] Y.L. Shoshin, M.A.Trunov, X.Y. Zhu, M. Schoenitz, E.L Dreizin. Combust. Flame 144 (2006):688-697

[9] J. Jellinek J (2008). Faraday Discussions 138 (2008):11-35

[10] Y. Wang,W. Jiang, X. Zhang,H. Liu, Y.Liu, F. Li. Thermochimica Acta 512 (2011):233-239.

[11] G. Rossi, R. Ferrando, C. Mottet, Faraday Discussions 138 (2008):193-210.

[12] L. Deng, H. Deng, S. Xiao, J.Tang, W Hu. Faraday Discussions. 162 (2013): 293-306

[13] E.L. Dreizin, Prog. Energy Combust. Science 35 (2009):141-167

[14] C. Holse, C F. Elkjaer, A. Nierhoff et al. The Journal of Physical Chemistry C 119 (5), 2015, 2804-2812

[15] N R Kim, K. Shin, I. Jung et al. The Journal of Physical Chemistry C 118, (2014), 26324-26331.

[16] Y. Aly, M. Schoenitz, E.L.Dreizin EL. Combust. Flame 160 (2013):835-842.

[17] G. Jian, S. Chowdhury, K.Sullivan, M.R. Zachariah MR, Combust. Flame 160 (2013):432-437.

[18] K. Sullivan, G. Young,M.R. Zachariah, Combust. Flame, 156 (2009):302-309

[19] R.Ferrando, J. Jellinek and R.L.Johnston. Chemical Reviews, 108 (2008): 848-910

[20] G Singh, I. Kapoor, S. Dubey. J Alloy Compd 480 (2009):270-274.

[21] E M. Abdelkader, P A Jelliss and S W Buckner Materials Chemistry and Physics, 2015, 149-150, 238-245

[22] A.Gromov, U. Forter-Barth and U. Teipel Powder Technology, 164 (2006): 111–115

[23] I. V. Beketov, A.P.Safronov, A.I. Medvedev, J. Alonso, G.V.Kurlyandskaya and S.M. Bhagat. AIP Advances 2 (2012): 022154

[24] K. Song, W.Kim, C. Suh, D.Shin, K.Ko and K. Ha. Powder Technology, 246 (2013): 572-574.

[25] W. Kim, J.S. Park, C. Suh, H. Chang and J.C.Lee, Materials Letters, 62 (2007): 4259-4261

[26] M K Berner, V E Zarko, M B Talawar, Combustion, Explosion, and Shock Waves, 49 (2013), 625-647

[27] P. Song, D.S. Wen, The Journal of Physical Chemistry C 113 (2009):13470-13476.
[28] P. Song, D.S. Wen,Z.X. Guo,T. Korakianitis T, Phys. Chem. Chem. Phys, 10 (2008):5057-5065.
[29] D.S.Wen, P.Song, K. Zhang, J. Chem. Tech. Biotech., 86 (2011): 375-380
[30] F.Noor, H.Zhang, T.Korakianitis, D.S.Wen, Phys. Chem. Chem.Phys,15 (2013): 20176-20188
[31] T.Uchikoshi, Y.Sakka, M.Yoshitake, K.Yoshihara. Nanostructured Materials 4 (1994):199-206.
[32] K.Wieczorek-Ciurowa, K.Gamrat, Z.Sawłowicz. J. Therm Anal Calorim 80 (2005):619-623
[33] V.M.Boiko, S.V.Poplavski. Shock Waves 11 (2002):289-295.
[34] M.A.Trunov, M.Schoenitz, E.L Dreizin EL. Combust. Theo.Modelling 10 (2006):603-623.
[35] V.Rosenband. Combust. Flame 137 (2004):366-375.
[36] V.I. Levitas, B.W.Asay, S.F. Son and M. Pantoya. *Appl Phys Lett* **2006**, *89*
[37] T.Tsuchida, R.Furuichi, T. Sukegawa, M.Furudate, T.Ishii. Thermochimica Acta 78 (1984):71-80.
[38] P.Bolt, F. Habraken, J.W.Geus, J. Solid State Chemistry 135 (1998):59-69.
[39] M.Arjmand, A.M.Azad, H. Leion, A. Lyngfelt, T.Mattisson, Energy & Fuels 25 (2011):5493-5502
[40] K.T. Jacob, C.B. Alcock, Journal of The American Ceramic Society 58 (1975):192-195.
[41] Y. Kumekawa, M. Hirai, Y. Kobayashi, S.Endoh, E.Oikaw, T. Hashimoto J Therm Anal Calorim 99 (2010):57-63.
[42] P.Bolt, F. Habraken, J.W.Geus, J. Solid State Chemistry 135 (1998):59-69.
[43] C.Y.Hu , K.Shih, J.O.Leckie. J. Hazardous Materials 181 (2010):399-404
[44] A. Ilyin, A.Gromov, V.An, F.Faubert, C.de Izarra, A. Espagnacq,L. Brunet L. Propellants, Explosives, Pyrotechnics 27 (2002):361-364.
[45] Gromov, A. Ilyin, U.Förter-Barth, U.Teipel. Propellants, Explosives, Pyrotechnics. 31 (2006):401-409
[46] D. Stamatis, Z. Jiang, V.K. Hoffmann, M. Schoenitz, E.L. Dreizin EL. Combust. Science and Technology 181 (2008):97-116

List of Figures

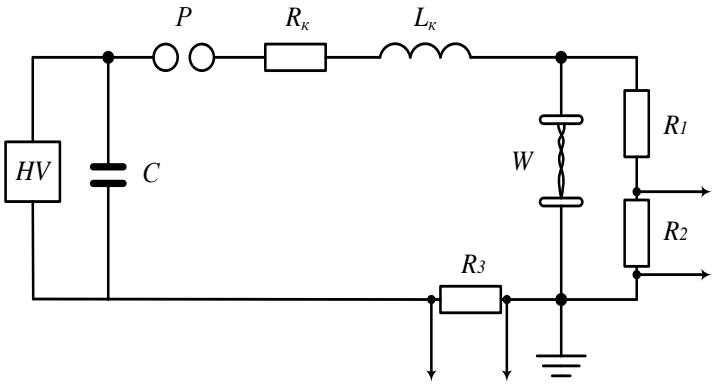

(a)

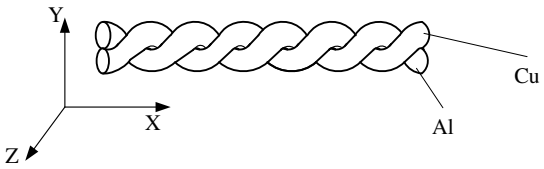

(b)

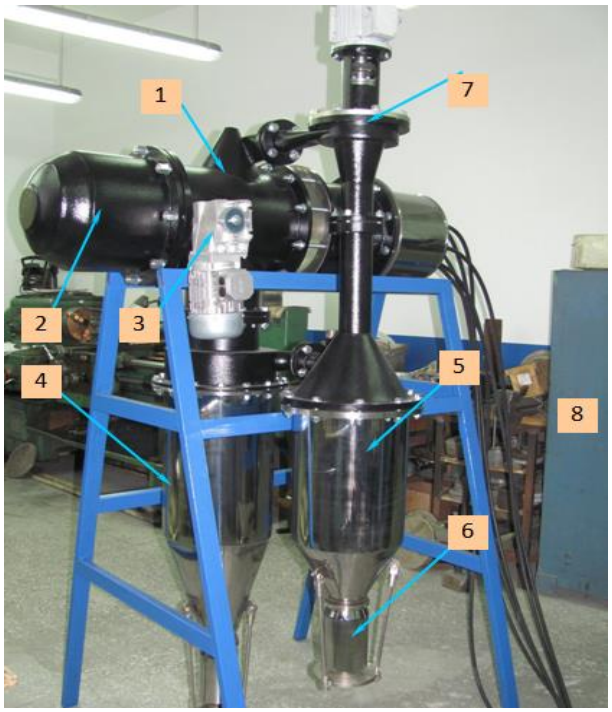

(c)

Fig. 1 Experimental setup: **a)** circuit diagram of nanopowder production unit (*HV* – high voltage power supply, *C* – capacitor bank, *P* – discharger for energy transmission from capacitor C to twisted wires *W*, $R_к$,$L_к$ – Ohmic resistance and inductance of the circuit, R_1 and R_2 – voltage divider for registering voltage impulse on *W*, R_3 – current shunt for registering current impulse through *W*); **b)** schematics of Cu-Al wires and **c)** snapshot of the experimental system (EEW chamber; 2 wire reel; 3 Gear box; 4, 1st-stage aerosol separator; 5, 2st-stage aerosol separator; 6, particle collector ; 7 argon gas centrifugal blower; and 8, high current impulse generator)

a)

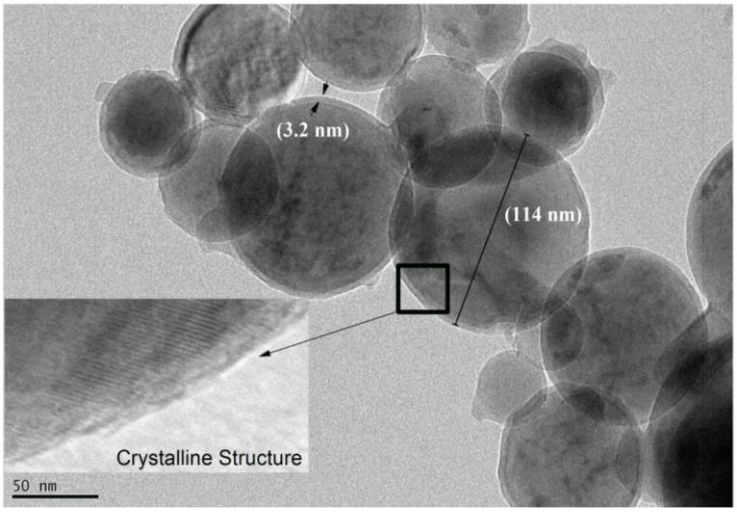

b)

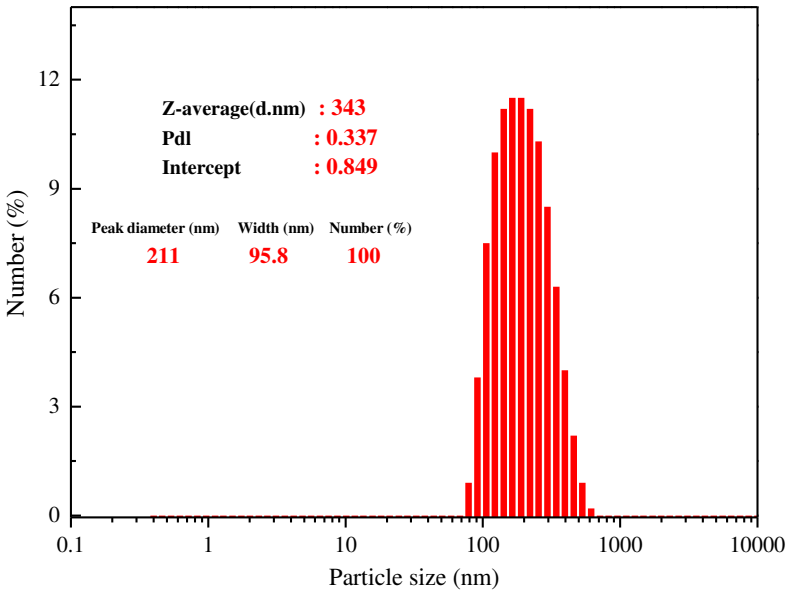

Fig. 2 Particle morphology, a) TEM image (*insert* enlarged view showing crystalline structure) shows the passivation layer, and b) DLS measures the particle size distribution (PSD) of nAlCu.

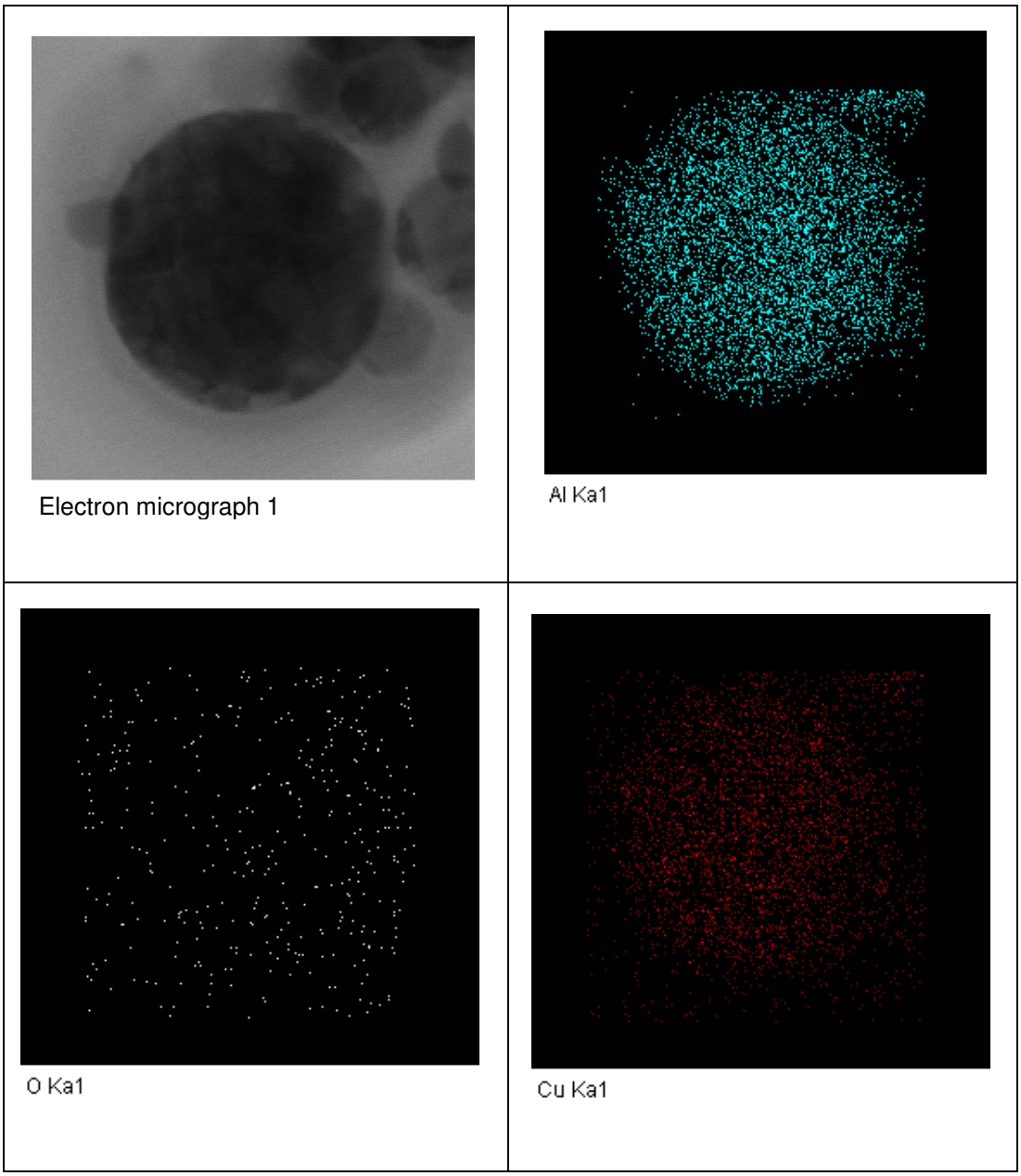

Fig.3 Distribution of elements (O, Al and Cu) in nAlCu particle (Initial Cu content - 20 %)

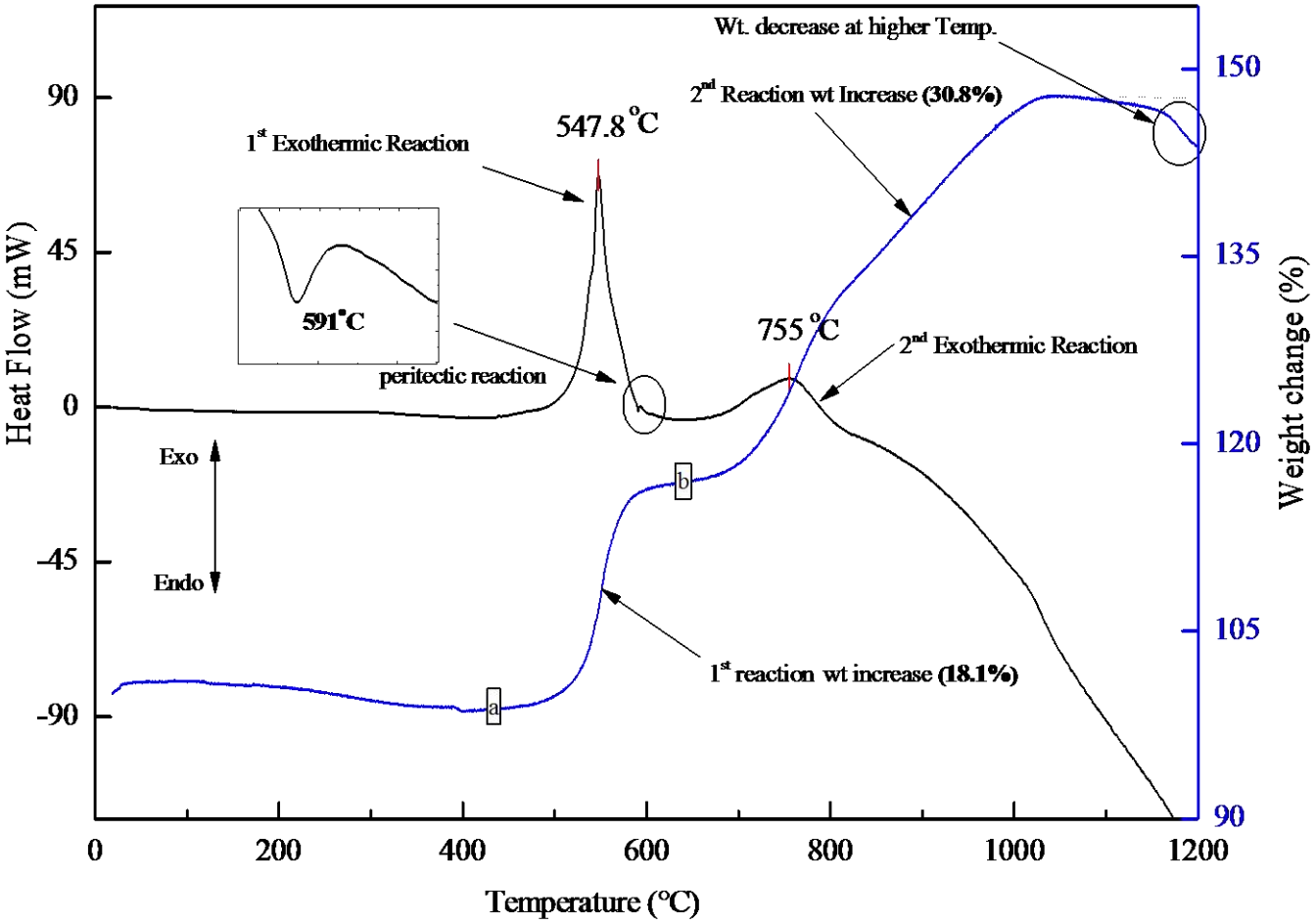

Fig. 4 Example TGA/DSC curve of nAlCu at 7 K/min (no ignition)

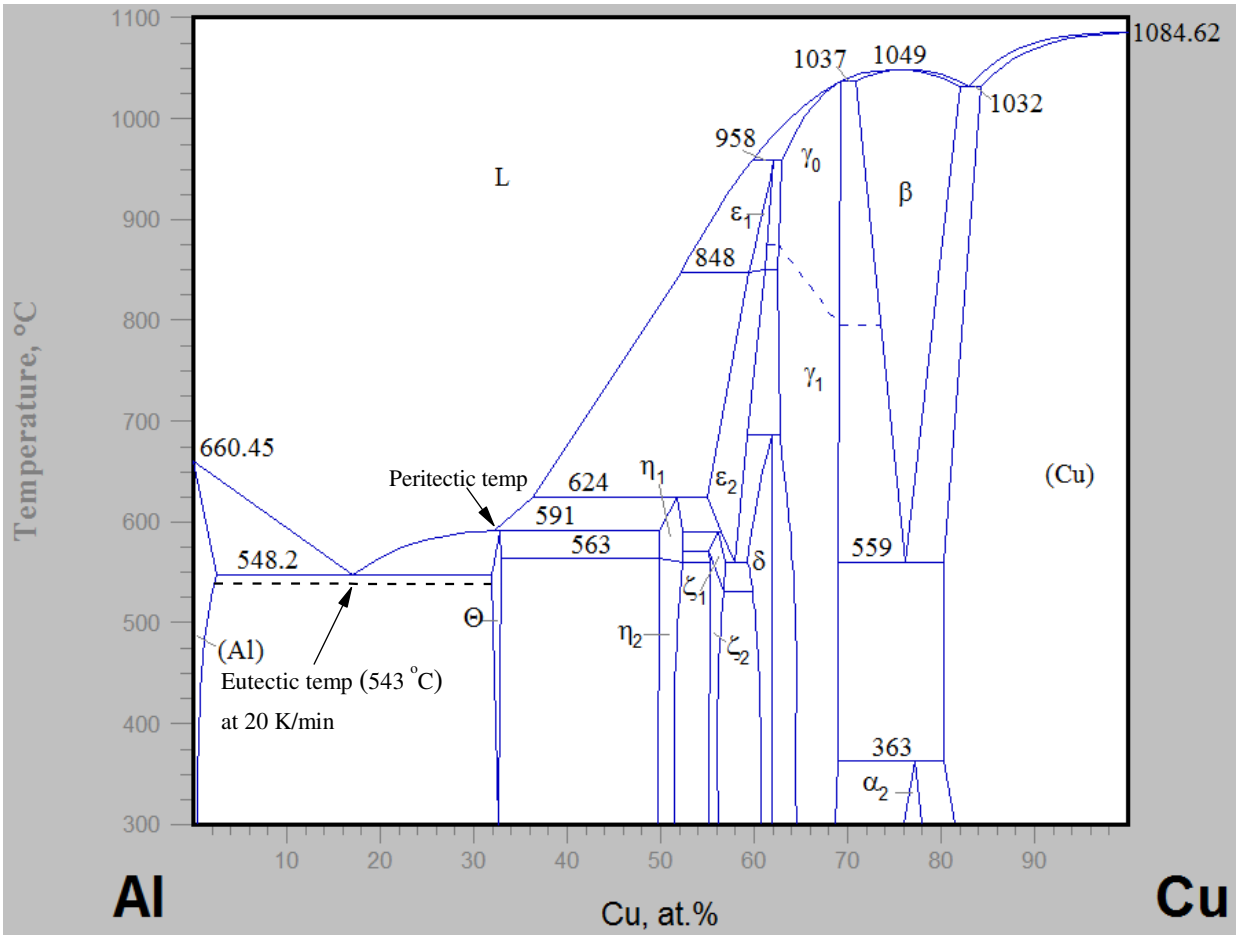

Fig. 5 Phase diagram of Al-Cu alloy binary system (Massalski 1990)

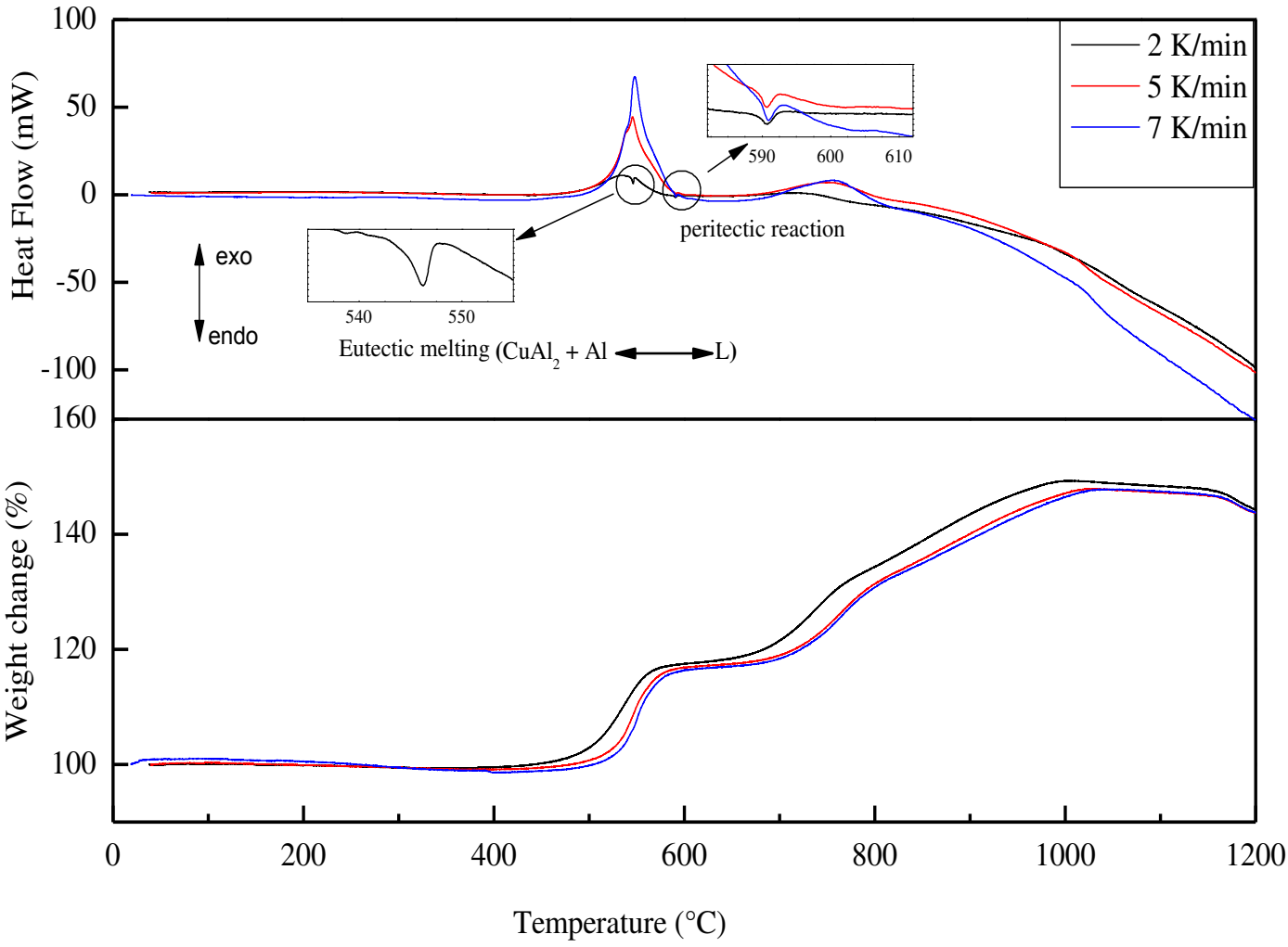

Fig.6 TGA/DSC of nAlCu at heating rates of 2-7 K/min (*inset* showing eutectic and peritectic reactions)

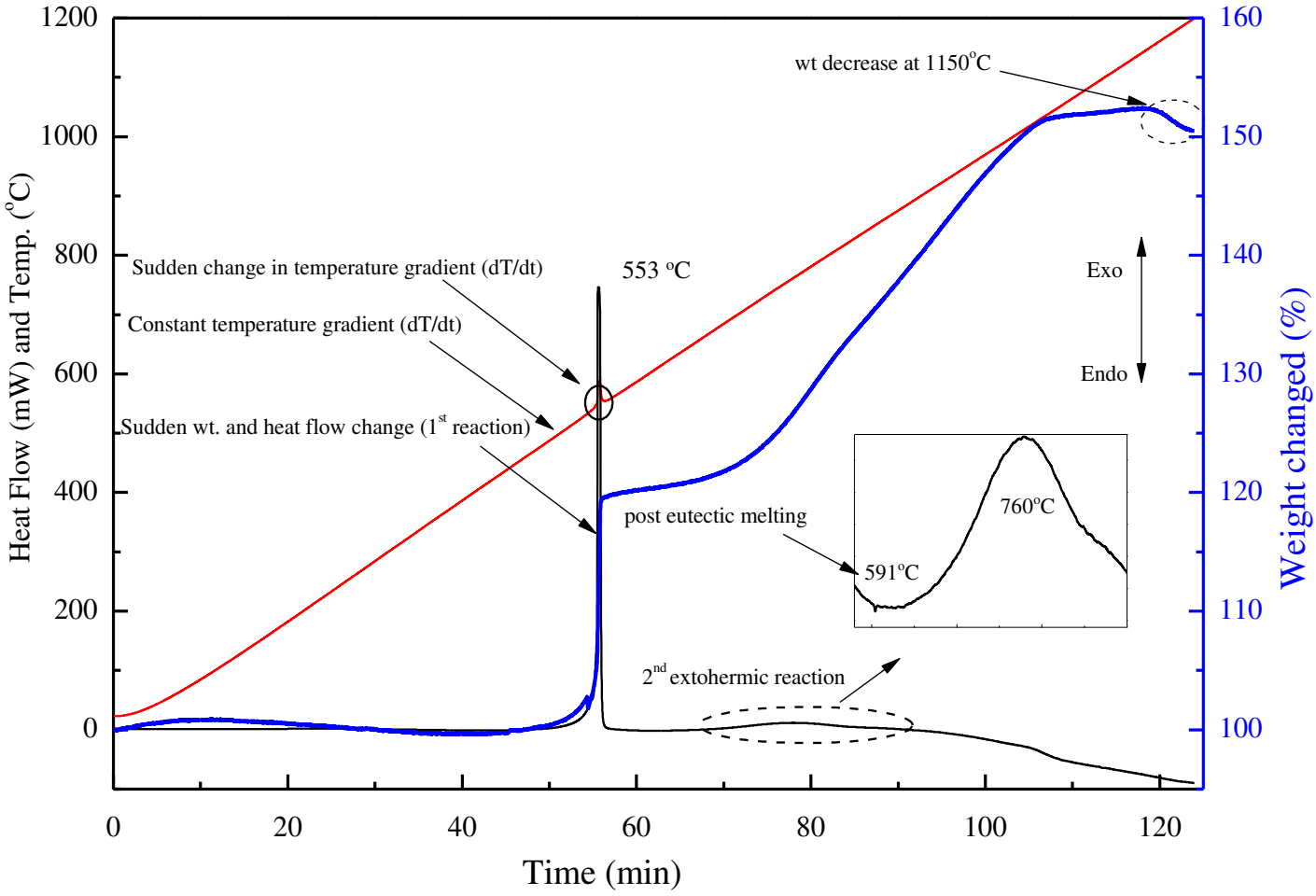

Fig.7 Example TGA/DSC of nAlCu at 10 K/min (*inset* showing peritectic reaction and 2nd exothermic reaction)

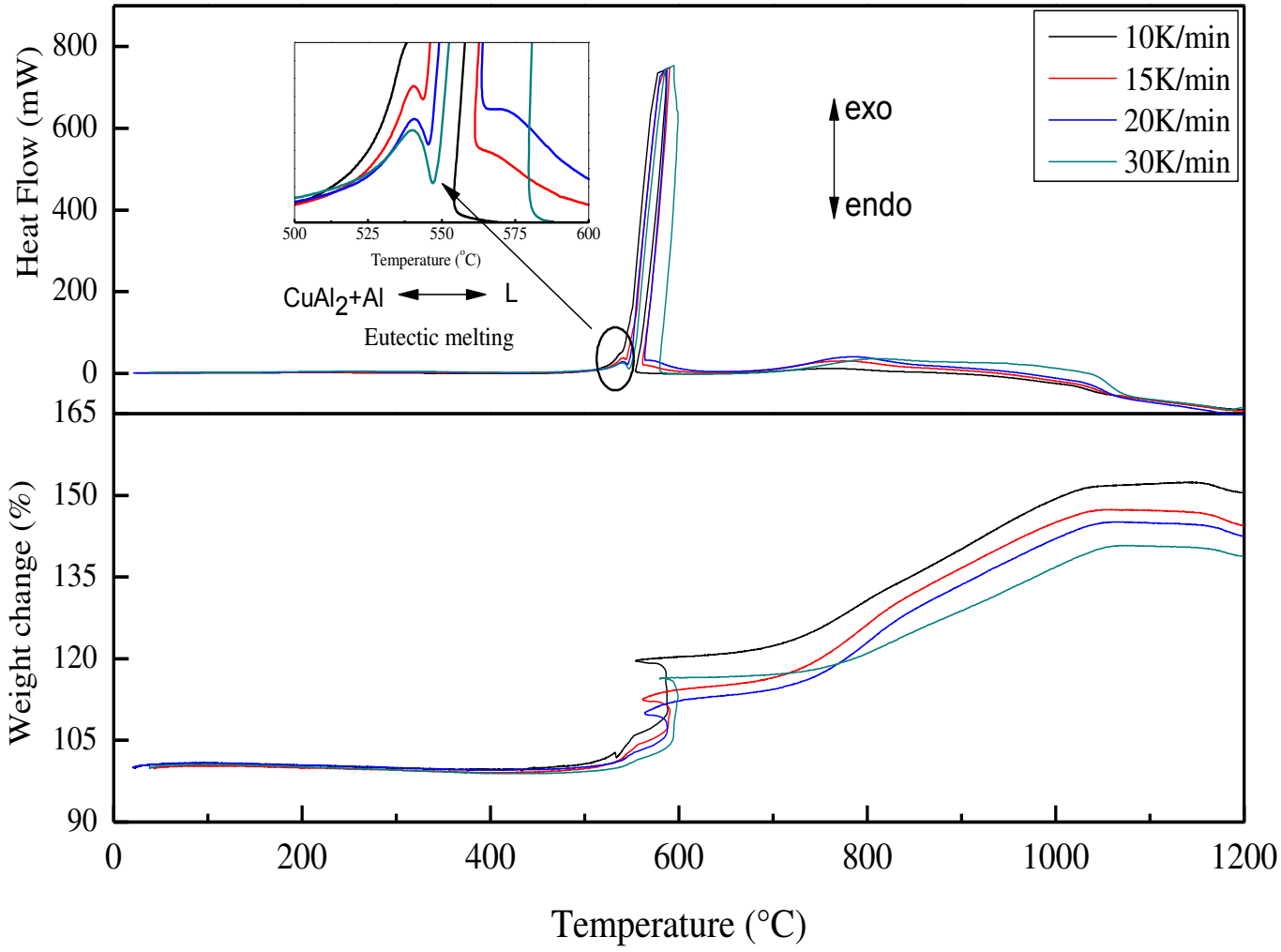

Fig. 8 TGA/DSC of nAlCu at heating rates of 10-30 K/min (*inset* showing eutectic melting reaction before the ignition)

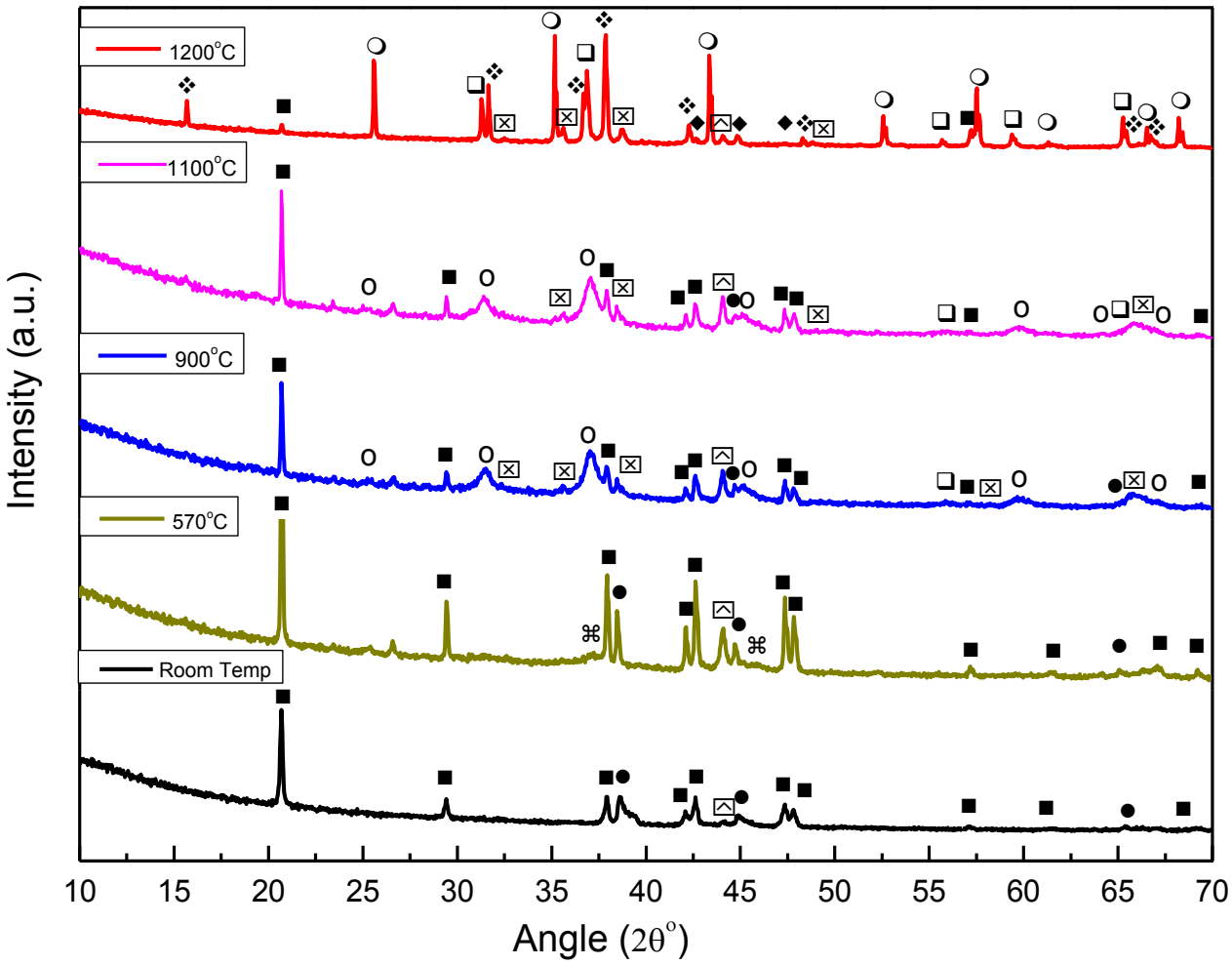

Fig. 9 XRD analyses of nAlCu at under various temperature conditions at10K/min (● Al, ■ $CuAl_2$, ❍ Al_2O_3, ☒ CuO, ❖$CuAlO_2$, ❑$CuAl_2O_4$, ⛥ Cu_9Al_4, o θ-Al_2O_3, ⌘δ-Al_2O_3, ⬥Cu_2O)

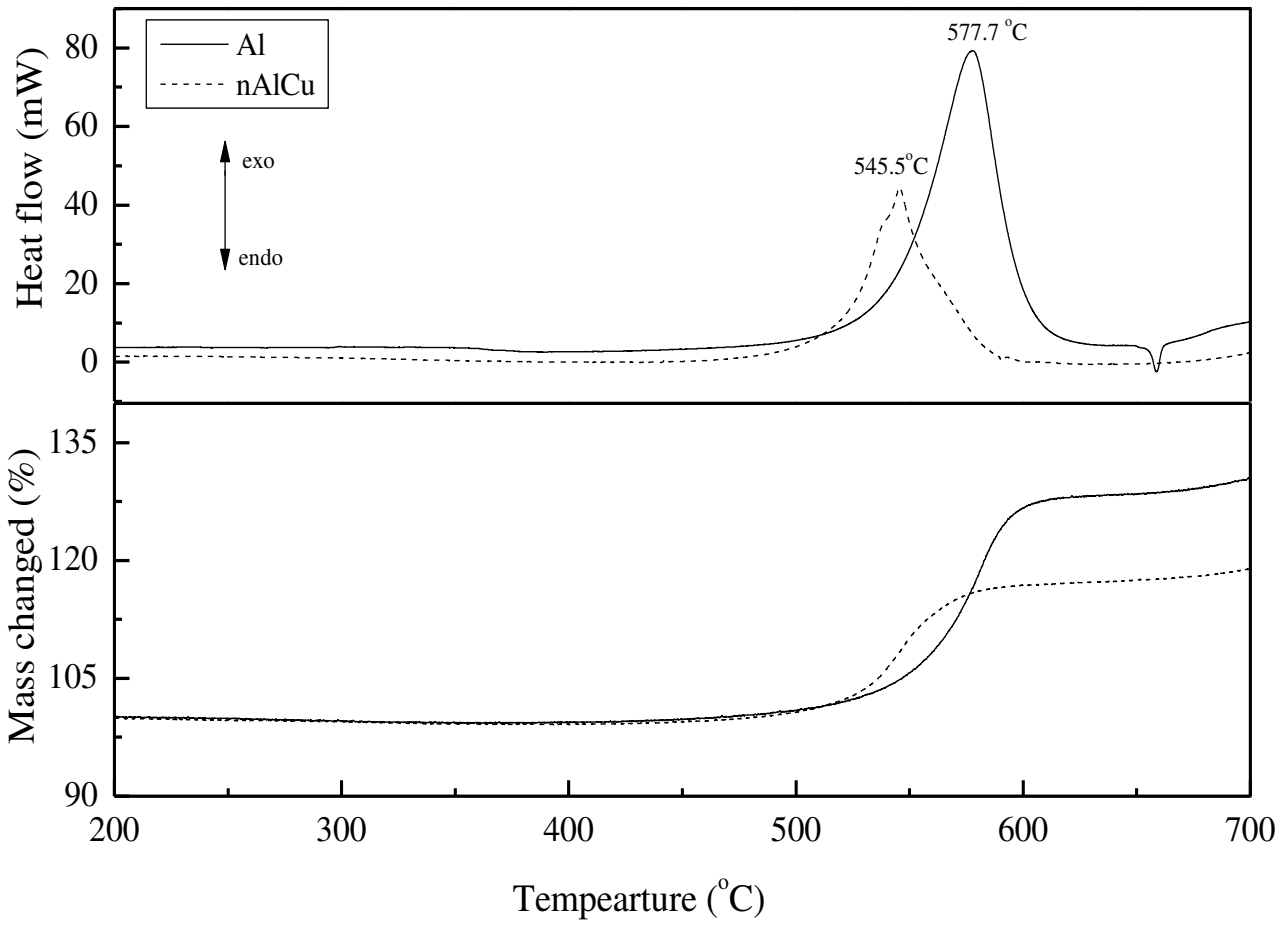

Fig. 10 TGA/DSC curves of nAl and nAlCu at a heating rate of 5 K/min showing nAlCu is more reactive

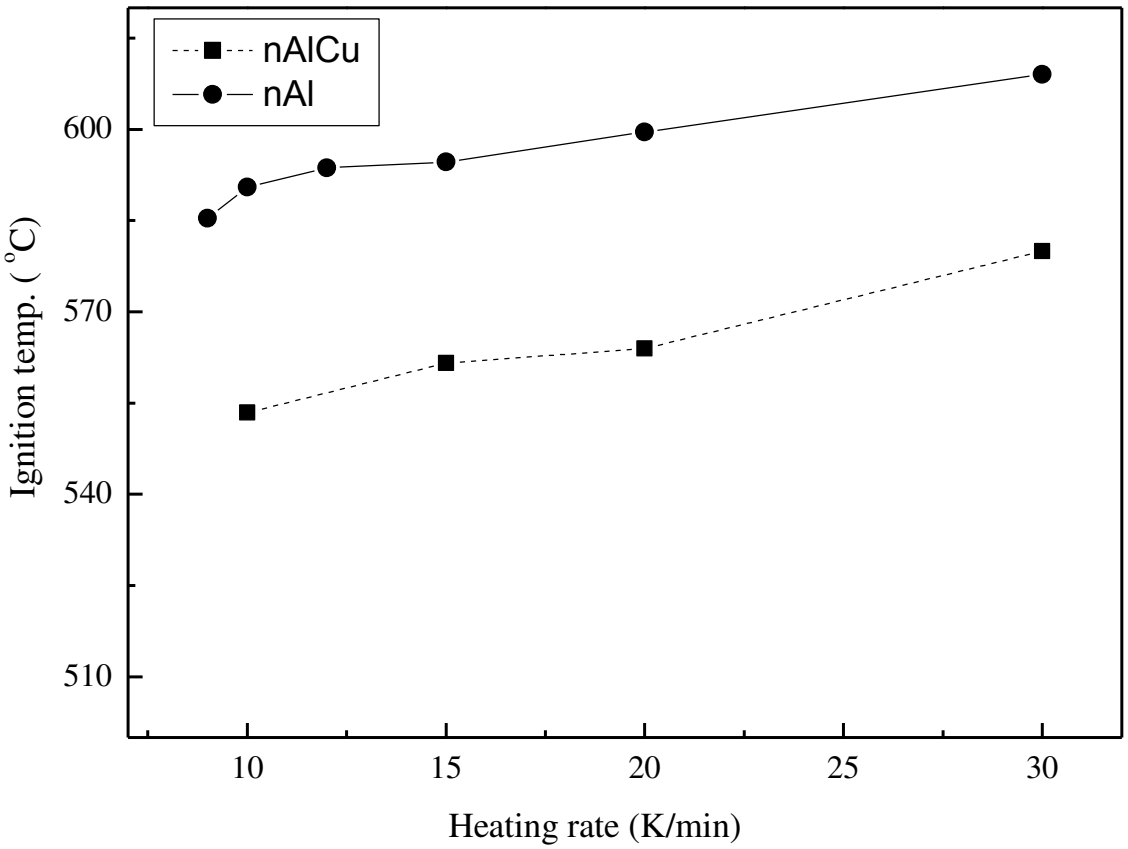

Fig. 11 Comparison of ignition temperatures of nAl with nAlCu showing nAlCu is ignited at lower temperature as compared to nAl under similar experimental conditions

Tables

Table. 1 EDS analysis of produced nAlCu from EEW method (SEM shows the location of the sampling)

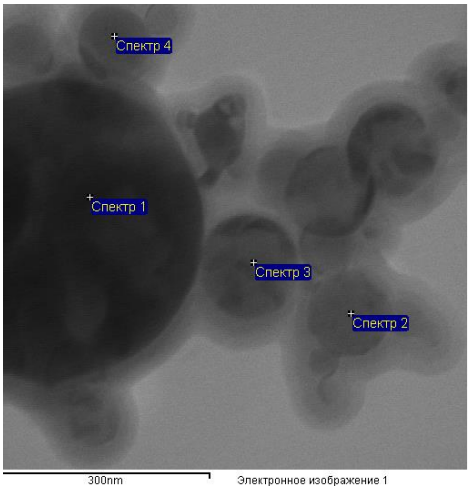

Element content in the point of analysis (atomic ratio)			
Spectrum	O, at. %	Al, at. %	Cu, at. %
Spectrum 1	7.72	68.15	24.14
Spectrum 2	25.43	57.42	17.15
Spectrum 3	22.41	58.79	18.80
Spectrum 4	29.29	46.36	24.35
Mean	21.21	57.68	21.11
Standard deviation	9.43	8.92	3.68
Max	29.29	68.15	24.35
Min	7.72	46.36	17.15

Table. 2 Reactivity parameters of nAlCu and nAl at 5 K/min

Sample	T_{onset}	T_{p1}	T_{m1}	T_{h1}
	^{o}C	^{o}C	^{o}C	^{o}C
nAlCu	528	545.5	547	533
nAl	551	577.7	578	567

Note: T_{onset} is the onset temperature; T_{p1} is peak temperature of the first exothermic reaction, T_{m1}= $(dm/dT)_{max1}$ and T_{h1}= $(dh/dT)_{max1}$ are the temperatures where the rate of change of mass and rate of change of heat are maximum.